Self-Assembly of Nanocolloidal Gold Films

E. Stefan Kooij
E. A. Martijn Brouwer
Agnes A. Mewe
Herbert Wormeester
Bene Poelsema
University of Twente, Enschede, The Netherlands

INTRODUCTION

The unique and new optical, electrical, and magnetic properties of colloidal superstructures as opposed to the bulk characteristics of the constituent materials is attracting the attention of an increasing number of both fundamental scientists and technology-oriented industry. The colloid size used in the assembled structures varies over approximately 3 orders of magnitude and is closely related to the specific application. For photonic band gap materials, the particle size is of the same order of magnitude as the wavelength of light, while for magnetic applications, such as ultrahigh density storage devices, the particle radius is in the low-nanometer range. A combination of the aforementioned physical properties of colloidal matter introduces even more exciting fields of research. Electron transport through monolayers of magnetic nanocrystals or tunable photonic band gap materials, both controlled by applying a magnetic field, are only two examples of the many possibilities.

Nanotechnology is characterized by a continuous decrease of feature sizes, e.g., in electronic devices. Top-down fabrication methods, such as the well-established photolithography techniques, are being pushed toward their physical limits. Increasingly more research effort is presently being devoted to bottom-up fabrication methods. Instead of reducing the size of much larger, bulk materials, as is done with photolithography in combination with etching techniques, the focus is turning toward building up superstructures of much smaller building blocks. Self-assembly of single molecules or nanocolloidal particles into larger arrangements, employing intrinsic, extrinsic, or even externally induced interactions, seems to be a most promising method, which is not hampered by problems related to scaling the processes to production scale. Much of the research activities in the field are focused on gold nanoparticles, as these systems are stable in a large number of environmental conditions and are relatively easy to prepare and control. In the first part of this contribution, we will summarize the different self-assembly methods with which nano-colloidal gold particles are composed into monolayers or multilayered superstructures.

In the second part of this contribution, we show how nonimaging, single wavelength reflectometry measurements can be applied to in situ study the formation of nanocolloidal gold monolayers at derivatized silicon surfaces. The kinetics of particles with dimensions in the low-nanometer range are investigated using a radial impinging jet setup, also referred to as a stagnation point flow geometry. We compare our results to similar adsorption experiments using micrometer-sized silica particles. For these large particles, the random sequential adsorption (RSA) model adequately describes the overall deposition kinetics. However, for considerably smaller particles in the 10–100 nm range, this relatively simple model fails. Here we show that a generalized adsorption model is in perfect agreement with deposition transients of particles in the low-nanometer range over the entire coverage range.

SELF-ASSEMBLY METHODS TO GROW NANOCOLLOIDAL GOLD FILMS

Many different ways have been employed to assemble colloidal particles into disordered structures or highly ordered superlattices. Most of these methods have also been applied to nanometer-sized gold particles, but because their size is orders of magnitude smaller than, for example, the particles used in photonic band gap applications, the results are often different.

One of the most frequently used methods, and without doubt the most often described[1–20] assembly technique, involves the chemical modification of the substrate onto which the nanocolloidal gold particles are adsorbed. Amino (NH_2)- and thiol (SH_2)-terminated surfaces lead to a high affinity for irreversible deposition of gold entities from solution. Additionally, the adsorption is self-limiting, as only submonolayer coverage can be achieved. Amino- or thiol-functionalized surface can be produced either by attaching aminosilane or thiolsilane molecules to

oxidic surfaces, such as silicon and aluminum oxide, or by adsorbing bifunctional amino–thiol or dithiol molecules onto gold substrates. In the latter case, short-chain molecules are used because long-chain molecules with a sufficient degree of freedom will attach to the gold surface with both ends. In most cases, immersion of the substrate into a solution of the functionalizing substance is adequate, but also evaporation/sublimation of the amino or thiol compounds is employed.

The interaction between the functional groups on the surface and the gold nanocrystals in solution is generally considered to be electrostatic, which enables relatively simple tuning of the surface potential by varying the pH of the solution. Once the gold particles are adsorbed on the substrate, the strong bonding, which is of a covalent character, prevents desorption. Also, the lateral mobility is negligible and the deposition is governed by a random sequential adsorption (RSA) process. For this reason, ordering does not take place and the spatial arrangement of the nanocrystals is random. The maximum surface coverage corresponding to an RSA event is approximately 55%.

To increase the coverage, e.g., to grown conducting gold layers, several routes can be taken. One of these involves the specific enlargement of the adsorbed gold nanoparticles by electroless deposition of gold or any other desired method. This seeded growth has been described in several publications.[9,10] In Fig. 1, we show scanning electron microscopy images of a monolayer of gold nanoparticles before and after seeded growth for 5 min in a $AuCl_4^-/NH_2OH$ aqueous solution. It is clear that the particles are enlarged to form a nearly percolating network. Additional growth leads to closed, conductive layers of gold.

Closely related to the aforementioned chemical functionalization of the substrates to enhance the specific affinity for gold nanoparticles is the use of DNA.[21,22] A major advantage of using DNA is that a specific network can be generated using specific DNA molecules. Thiol-terminated DNA molecules can be built into the structure; the location and the density can be determined by the ratio of various DNA types in solution.

As mentioned above, specific functionalization of the surface onto which the gold entities are adsorbed limits the coverage to submonolayer values. To overcome this restriction, the layer-by-layer (LBL) technique can be employed.[3,5,6,9,11–13,17,18,23–25] For example, adsorbed gold nanoparticles can be covered with a layer of cross-linker molecules, such as amino–thiols or dithiols. One end of these molecules attaches to the gold nanocrystal surface, while the other end generates new functionalized adsorption sites for additional colloidal particles. Not only the aforementioned chemical interaction can be used in LBL deposition, but also electrostatic interactions
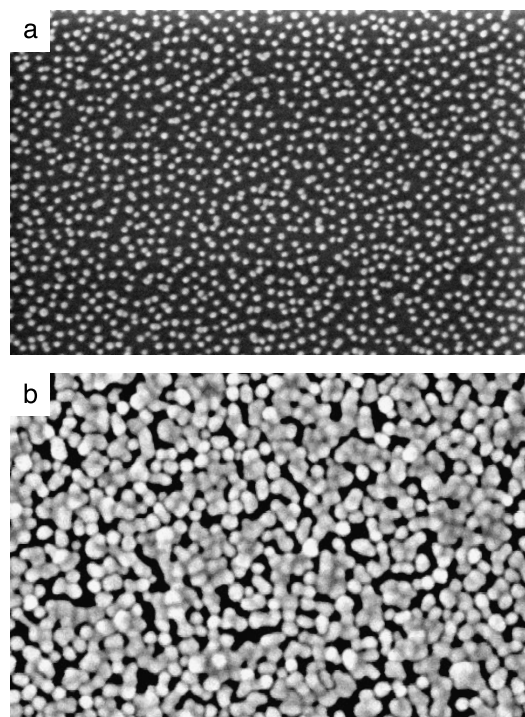

Fig. 1 Scanning electron microscopy images of colloidal gold particles irreversibly adsorbed at silicon/silicon oxide substrates, derivatized with APTES. The image size amounts to 1200 nm × 800 nm. Prior to seeded growth (a), the average spacing between the isolated nanocrystals is tunable via the ionic strength. Seeded growth for 5 min in a $AuCl_4^-/NH_2OH$ aqueous solution (b) gives rise to homogeneous particle enlargement.

are employed to form multilayers of gold nanoparticles. In this case, the cross-linker entities are polyelectrolyte molecules, or oppositely charged nanoparticles. In principle, the number of deposition cycles, and therewith the thickness of the superstructure, is not restricted. However, the roughness of the structure substantially increases, which limits the application in many cases.

The aforementioned derivatization, either chemical or electrostatic, of the substrate enables patterning of the substrate and thus also of the superstructure of nanocolloidal gold particles.[12,19,26,27] Examples of ways to locally functionalize substrates include microcontact printing and scanning probe microscopy (SPM)-based methods. In the former case, a polydimethylsiloxane (PDMS) stamp is generally used to apply the amino–thiol molecules or polyelectrolytes to predefined areas on the substrate surface. After rinsing, the gold nanocolloidal particles adsorb only onto the derivatized patterned regions. With SPM, the approach is somewhat different. A surface is completely functionalized with, for example, amino end-groups. Subsequently, specific regions on the surface are defunctionalized by oxidizing or removing the molecules,

therewith destroying the local affinity of the surface for gold adsorption. Although it allows complicated patterns to be made, the latter method is intrinsically slow as all structures have to be ''written'' onto the surface.

A completely different method used to form dense monolayers of gold nanoparticles is by electrophoretic deposition.[27–30] An external electric field is applied to drive the particles toward the surface. Although very impressive results have been obtained for micrometer-sized colloidal systems, the work on nanocolloidal gold particles is limited to a few reports of experimental results. In principle, highly ordered monolayers, and possible also multilayers, can be formed as the lateral mobility of the gold nanocrystals is not hindered.

Finally, hydrodynamic interactions can also be employed to form superstructures of gold nanoparticles.[4,16,31–33] The simplest approach is to simply dry the colloidal suspension on a substrate. This already generates a short-range order in the deposited layers. Control over the spatial extent of the ordering can be achieved by lowering the evaporation rate of the solvent, therewith giving the particles the opportunity to find a suitable spot in the superstructure while it is forming. The volume fraction also plays an important role. Modifications of this method, specifically for gold nanoparticles, have been described. The nanocrystals are first adsorbed onto amino- or thiol-derivatized surface, after which they are ''liberated'' by a ligand-exchange reaction. This is considered to increase the lateral mobility of the particles on the surface, which then allows them to ''dry'' in an ordered monolayer.

KINETICS OF IRREVERSIBLE GOLD NANOCRYSTAL DEPOSITION

A prerequisite for studying any system in general, but nanocolloidal systems in particular, is the ability to unambiguously characterize them under relevant conditions. Among the large number of methods available for characterizing colloids and their superstructures, electron microscopy [scanning electron microscopy (SEM)/transmission electron microscopy (TEM)] is by far the most popular. Both for very small as well as relatively large particles, this encompasses the most employed ex situ technique. Among colloid scientists, the use of scanning probe microscopy [atomic force microscopy (AFM), scanning tunneling microscopy (STM), magnetic force microscopy (MFM)] is increasing, but also in this case experiments are typically performed ex situ. In fact, the only techniques that have been used in situ to study colloidal systems are optical methods. Imaging techniques such as conventional or confocal microscopy are used for large colloids. For particles with dimensions well below

the diffraction limit of (visible) light, such as with gold nanoparticles, only nonimaging (lateral averaging) in situ experiments are available. These include primarily UV/vis absorption spectroscopy, but also optical waveguide light-mode spectroscopy, and reflection techniques as reflectometry and ellipsometry.

Single Wavelength Reflectometry Results

We employed single wavelength reflectometry to characterize the adsorption of nanocolloidal gold particles onto substrates derivatized with aminopropyltriethoxysilane (APTES).[20] Gold colloids are prepared by standard citrate reduction of $HAuCl_4$ in aqueous solution at $100°C$, which yields colloidal particles with an average radius of $a = 6.7$ nm.[15] In all our reflectometry measurements, the as-prepared nanocolloidal gold suspension is diluted by a factor of 4, which leads to a particle concentration of approximately $c_0 = 1.85 \times 10^{18}$ m^{-3} and an ionic strength of 3.6 mM.

The homebuilt reflectometer setup consists of a He–Ne laser, the stagnation point flow cell, a beamsplitter, and two photodiodes for detecting the intensities I_p and I_s of the parallel and perpendicular components of the reflected light. A more extensive description of our specific setup is given by Dijt et al.[34] The intensity ratio $S = I_p/I_s = (I_{0p}/I_{0s})(R_p/R_s)$ is measured, where I_{0p} and I_{0s} are the initial intensities and R_p and R_s are the intensity reflection coefficients. The angle of the incident beam can be adjusted and is set to $71°$ with respect to the normal of the sample surface. The volume flow during the experiments was approximately 1.0 mL min^{-1}.

For the reflectometry experiments, we used substrates cut from p-type silicon (100) wafers with a deposited oxide layer of 45 nm. When the oxide layer is too thin, R_p is very small and the initial sensitivity of the setup is low. With too thick oxide layers, the reflectometer signal flattens and even decreases above a certain surface concentration. The reflectometer signal has been calculated as a function of the gold nanocrystal coverage using the thin island film theory;[35,36] the relation between signal and coverage is used as a calibration to obtain an absolute surface coverage from the optical response.

In Fig. 2, we show typical reflectometry transients, obtained during colloidal gold deposition in the aforementioned stagnation point flow cell at various ionic strengths. For $t < 0$, only water flows through the cell, and a constant baseline is measured. At $t = 0$, the gold suspension is injected into the cell. When the flow is switched back to water at $t = 38$ min, no significant decrease of the surface coverage is observed, indicating the absence of particle detachment. Two distinct regimes are observed in the measured curves in Fig. 2, which will be discussed in the next section.
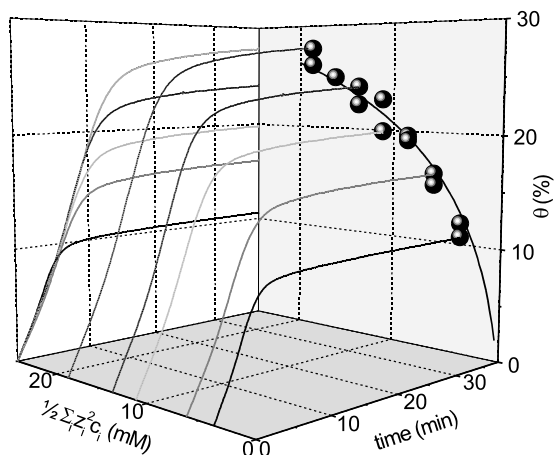
Fig. 2 Three-dimensional representation of the ionic-strength-dependent adsorption kinetics of gold nanocolloidal particles in stagnation point flow geometry. The coverage is obtained by polarized reflectometry. The data on the back panel indicate the evolution of the saturation coverage with increasing ionic strength for a number of reflectometry experiments; the solid line is a guide to the eye.

Two Limiting Regimes in the Deposition Transients

At longer deposition times, the deposition process leads to saturation at coverage values, which show a clear dependence on the ionic strength.[15] This will be discussed at the end of this section. For short times, the deposition rate is similar for all ionic strengths, which implies that the deposition process is initially limited by the supply of colloidal particles to the surface. The hydrodynamics of colloid deposition in a stagnation point flow cell have been extensively described.[37,38] The initial particle flux toward the surface is in good approximation given by

$$j_0 = 0.776 c_0 \left(\frac{D^2 \alpha V_m}{R^2} \right)^{\frac{1}{3}} = k_c c_0 \qquad (1)$$

where c_0 is the bulk particle concentration, D is the diffusion coefficient of the nanocolloidal particles, $R = 0.64$ mm is the radius of the inlet tube and $V_m = v \cdot Re/R$ is the average flow velocity, with Re the Reynolds number and v the kinematic viscosity of the fluid. The dimensionless flow parameter α depends on the Reynolds number and the cell geometry parameter h/R. In our case, a value $\alpha = 4.2$ is obtained from the work of Dabros and Van de Ven[37] using $Re = 8.3$ and $h/R = 1.7$. The mass transfer coefficient k_c will be discussed in a later section.

Assuming pure random sequential adsorption (RSA), with a sticking probability of 1, the above considerations imply a constant deposition rate $d\theta/dt$ from the moment the colloidal suspension is inserted. After a short transition time, this linear regime is indeed observed. The adsorption rate $d\theta/dt = \pi a^2 j_0 = 0.0225$ min^{-1} in Fig. 2 is used to calculate the particle diffusion coefficient D from Eq. 1. For lower ionic strengths, the value of D is less accurate but within an experimental error of 5%, the aforementioned value $d\theta/dt = 0.0225$ min^{-1} does not vary with ionic strength. Inserting the known values for particle density and cell geometry parameters, we find $D = 6.9 \times 10^{-12}$ m^2 sec^{-1}. We now compare this result to the diffusion coefficient obtained using the Stokes–Einstein relation

$$D = \frac{kT}{6\pi \eta a} \qquad (2)$$

where kT is the thermal energy and η is the dynamic viscosity of the fluid (for water, $\eta = 1.00 \times 10^{-3}$ kg m^{-1} sec^{-1}). With a particle radius $a = 6.7$ nm, the Stokes–Einstein relation yields a diffusion coefficient $D = 3.2 \times 10^{-11}$ m^2 sec^{-1}. Our experimentally determined value is about 4–5 times lower than this value. The apparent discrepancy is reasonable, considering the following arguments. One reason is that Eq. 2 represents an approximation[38] that is only valid in the infinitely small stagnation point in the center of the cell, whereas an elliptical area of about 1×2 mm^2 is probed in the experiments. From SEM data, Böhmer et al.[39] estimated that in the initial stage of nanocolloidal film growth, the adsorption rate is underestimated by a factor of 1.5. Numerical calculations based on the flow field in the cell[38] confirm that indeed the average flux on a probe area of 1×2 mm^2 is approximately $0.7 j_0$. This implies an underestimation of the diffusion coefficient D in our experiments by approximately a factor of 2. Furthermore, the gold nanocolloids have a relatively large surface charge, which leads to an increased hydrodynamic radius, and thus a lower diffusion constant (Eq. 2). The particle concentration has been determined to have a small error, so we do not believe this interferes with our determination of the diffusion coefficient.

Let us now turn to the saturation regime of the deposition curves in Fig. 2. For higher ionic strengths, the maximum attainable coverage increases, in agreement with the Derjaguin-Landau-Verwey-Overbeek (DLVO) theory. This theory describes the accumulation of ions near charged interfaces, in this case the colloid–solvent interface, which results in a double layer around every particle. When the double layers of two particles overlap, the ions around the particles are confined to a smaller volume, which results in an entropic repulsion. This repulsion prevents coagulation of the particles, and also defines the distance of closest approach of two particles.

When particles adsorb on a surface, this distance determines the maximum attainable coverage.[15]

More quantitatively, the double-layer interaction potential $U_{pp}(r/a)$ in units kT is described by,[40,41]

$$\frac{U_{pp}\left(\frac{r}{a}\right)}{kT} = B_{pp}\frac{a}{r}e^{-\kappa(r-2a)} \qquad (3)$$

where r is the particle–particle distance and κ is the Debye screening parameter, given by

$$\kappa^2 = \frac{e^2 \sum_i n_i z_i^2}{\varepsilon\varepsilon_0 kT} \qquad (4)$$

with n_i and z_i being the number density and valence of ions i, respectively, e the elementary charge, and $\varepsilon\varepsilon_0$ the dielectric permittivity of the electrolyte. The particle–particle interaction coefficient is defined as

$$B_{pp} = \left(\frac{4\pi\varepsilon\varepsilon_0 kTa}{e^2}\right)\left(\frac{y_p + 4\gamma\Omega\kappa a}{1 + \Omega\kappa a}\right)^2 \qquad (5)$$

with $\gamma = \tanh(y_p/4)$, $\Omega = [(y_p - 4\gamma)/2\gamma^3]$, and $y_p = \psi_p(e/kT)$ the dimensionless surface potential. This yields an interaction potential that is valid over a large range of κa provided r is larger than about $a + (3/2)\kappa^{-1}$. Assuming a constant surface potential, the distance r_{kT} between particles when their interaction energy drops below $(3/2)kT$ can be numerically determined as a function of κa, i.e., as a function of the ionic strength. The choice for the interaction energy is justified by the fact that particles have an average thermal energy of $(3/2)kT$, which competes with their electrostatic repulsion upon approaching each other.

In Fig. 3, the saturation coverage θ_{calc}, calculated using Eqs. 3–5 with a particle surface potential $y_p \cdot kT/e = -85$ mV,[42,43] is plotted as a function of the surface concentration θ_{meas} obtained from Fig. 2. The calculated coverage is obtained from the double-layer thickness defined as $\Delta a = r/2 - a$. Using the thus determined effective double-layer thickness Δa, the saturation coverage θ_{calc} is obtained from

$$\theta_{sat} = \theta_{jam}\left(\frac{a}{a + \Delta a}\right)^2 \qquad (6)$$

in which $\theta_{jam} = 54.7\%$ represents the jamming limit for irreversible random deposition of hard spheres.[41,44,45]

The data in Fig. 3 exhibit a good one-to-one relation between experiment and the DLVO theory. However, at large values of the ionic strengths and thus high surface concentrations, the measured coverages are higher. One
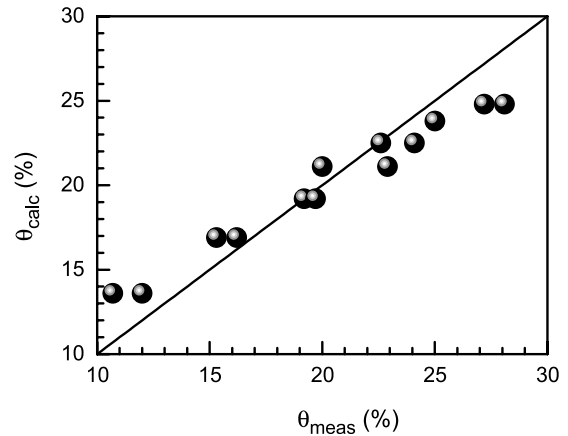

Fig. 3 Saturation coverage θ_{calc} calculated from the ionic strength using the DLVO theory as a function of the experimentally determined maximum coverage θ_{meas} from the reflectometry measurements. The line has a slope of 1.

cause is that the linear approximation of the Poisson–Boltzmann equation underestimates the potential drop near the particles. When a far-field potential is used, as it is here, the potential at short distances is overestimated. This results in an overestimation of the distance where the particle–particle interaction drops below $(3/2)kT$, and consequently leads to an underestimation of the surface concentration. The effect will become important when $r < a + (3/2)\kappa^{-1}$, which is approximately 10 nm for the highest ionic strengths. This value corresponds to a surface coverage of 25%, which is approximately the value at which the data in Fig. 3 start to deviate from the one-to-one relation (the solid line). Another possible explanation for the deviation at higher ionic strengths may be the formation of clusters on the sample surface. A cluster has a larger volume on a relatively small area, thereby accounting for a larger optically determined surface concentration.

Modeling the Deposition Transients

The deposition kinetics of colloidal particles can be described in terms of the adsorption rate $d\theta/dt$ by

$$\frac{d\theta}{dt} = \pi a^2 j_0 B(\theta) \qquad (7)$$

where πa^2 is the geometrical particle surface area and j_0 represents the limiting deposition flux for uncovered surfaces. The quantity $B(\theta) = j(\theta)/j_0$, with $j(\theta)$ being the actual deposition flux for a given coverage, is usually referred to

as the overall kinetic blocking function. This designation is somewhat misleading as $B(\theta)=1$ for low coverages, while in the limit of saturating coverages $B(\theta) \rightarrow 0$; so in fact $B(\theta)$ represents an effective, coverage-dependent available surface. More correctly, it is also referred to as the ''available surface function.''[46] The function $B(\theta)$ not only depends on the coverage, but also on many additional factors such as particle–particle interactions, the mechanism of particle transport, and the reversibility of particle adsorption.

In principle, the overall kinetic blocking function can only be determined empirically from the particle deposition rate as a function of time, i.e., curves similar to those presented in Fig. 2. If we assume that all deposition transients for our system (nanocolloidal gold particles irreversibly deposited on APTES-derivatized silicon oxide surfaces) are characterized by a single, coverage-dependent overall kinetic blocking function $B(\theta/\theta_{sat})$, where θ_{sat} is the saturation coverage defined in Eq. 6, the general adsorption Eq. 7 can be rewritten in terms of the dimensionless variables

$$\bar{\theta} = \theta/\theta_{sat} \tag{8a}$$

$$\bar{t} = \frac{\pi a^2 j_0}{\theta_{sat}} t \tag{8b}$$

to yield

$$\frac{d\bar{\theta}}{d\bar{t}} = B(\bar{\theta}) \tag{9}$$

The result of this scaling, applied to the deposition curves in Fig. 2, is shown in Fig. 4 where we have plotted the data according to Eq. 9. Apart from the initial first minutes (not shown in Fig. 4), it is clear that all curves collapse to a
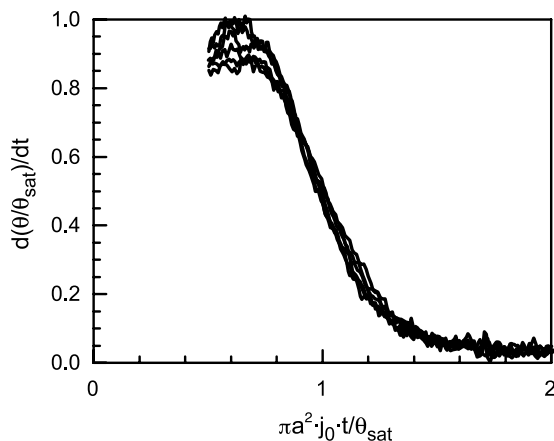

Fig. 4 Deposition transients of Fig. 2, scaled according to Eq. 9, using the dimensionless variables $\bar{\theta}$ and $\bar{t}$ as given by Eqs. 8(a) and 8(b).

single curve, verifying that indeed a single overall kinetic blocking function governs the deposition process, irrespective of the ionic strength.

A Generalized Adsorption Model

A theory, which is more specifically applicable to our system of colloidal particles, irreversibly deposited under forced convection conditions (stagnation point flow geometry), has been extensively described by Adamczyk.[47,48] A similar model was also described by Faraudo and Bafaluy.[49] In this generalized adsorption model, the deposition is considered to consist of two processes, i.e., 1) the actual adsorption, and 2) the convective supply of nanocrystals to the surface. The convective supply of colloidal particles to the outer edge of the adsorption layer, at a distance δ_a from the surface, is described by the rate constant $k_c = j_0/c_0$, where j_0 is equal to the particle flux. For the well-defined flow conditions in our stagnation point flow setup, k_c is given by Eq. 1.

The adsorption process is described by

$$\frac{d\theta}{dt} = \pi a^2 k_a c(\delta_a) B'(\theta) \tag{10}$$

and is governed by a rate constant k_a and a particle concentration $c(\delta_a)$ at distance δ_a from the surface.[50] The available surface function $B'(\theta)$, also often referred to as the generalized blocking function, describes the transport resistance of the adsorbed layer to adsorbing particles; effectively, it is equal to the overall sticking probability. In fact, Eq. 10 is similar to Eq. 7, in which the actual adsorption process is taken into account by the overall kinetic blocking function $B(\theta)$ considering a constant supply of colloidal particles. In Eq. 10, the adsorption process is considered and the supply of colloidal particles is described by the time dependence of $c(\delta_a)$. Within the adsorption layer of thickness δ_a, convection effects can be neglected. The thickness δ_a is comparable to the range of specific interactions, in principle electrostatic interactions, the extent of which is governed by the double-layer thickness. For our nanocolloidal particles, this implies that δ_a is of the same order of magnitude as the particle radius.

For the irreversible adsorption of particles at uniformly accessible surfaces, Adamczyk[47] derived an expression for the kinetic overall blocking function, given by

$$B(\theta) = \frac{KB'(\theta)}{1 + (K-1)B'(\theta)} \tag{11}$$

where $K = k_a/k_c$ represents the coupling between adsorption and convection processes. In the case of strong particle–particle interactions, $B'(\theta)$ can be approximated by the RSA available surface function $B_0(\theta)$. It is not possible

to analytically evaluate $B_0(\theta)$, but a good approximation is given by[47,51]

$$B'(\theta) = \left[1 + 0.812 \frac{\theta}{\theta_{sat}} + 0.426 \left(\frac{\theta}{\theta_{sat}} \right)^2 \right.$$
$$\left. + 0.0716 \left(\frac{\theta}{\theta_{sat}} \right)^3 \right] \left(1 - \frac{\theta}{\theta_{sat}} \right)^3 \qquad (12)$$

With this expression, the overall kinetic blocking function $B(\theta)$ can be calculated, using Eq. 11, which now only depends on the maximum coverage θ_{sat} obtained after saturation and the coupling constant K.

In practice, $K \sim 1$ for micrometer-sized particles.[47] However, our colloidal particles are markedly smaller, which leads to a significant increase of the value of K. This can be understood by considering that from Eq. 2, D is inversely proportional to the particle radius a. Therewith the convective flux, expressed by the rate constant k_c in Eq. 1, varies as $a^{-2/3}$. An analytical expression for the adsorption constant k_a is given by Adamczyk and Szyk[52]

$$k_a = \frac{D}{2a} \frac{1}{1 + \frac{1}{2} \ln \left(1 + \frac{\Delta a}{a} \right)} \qquad (13)$$

where Δa represents the extent of the repulsive interactions, i.e., the effective thickness of the double layer. With Eq. 2, we obtain for the coupling constant $K = k_a/k_c \sim a^{-4/3}$; that is, for smaller particles, K is expected to become considerably larger than 1.

In Fig. 5a, the coverage dependence of the overall kinetic blocking function is plotted for different values of K. A large value of K ($\gg 1$) implies that the adsorption rate is considerably larger than the convective supply of particles. Thus up to relatively large coverages, the deposition is transport-limited, which is expressed by the considerable coverage range over which $B(\theta/\theta_{sat}) \approx 1$. Only near the saturation coverage, $B(\theta/\theta_{sat})$ rapidly drops to 0. In the opposite case when $K = 1$, corresponding the pure RSA, the adsorption itself becomes rate-limiting. Accordingly, for low K values, $B(\theta/\theta_{sat})$ exhibits a sharp decrease already at low coverages.

From the deposition curves in Fig. 2, it is obvious that for a large coverage range, the deposition is dominated by mass transport of particles to the adsorption layer. The deposition rate $d\theta/dt$ only decreases upon approaching the saturation coverage. This indicates that for our system of nanocolloidal gold particles, irreversibly deposited in a stagnation point flow geometry, K is considerably larger than 1. To obtain more quantitative information, we fitted the generalized adsorption model, expressed by Eqs. 7, 11, and 12, to the deposition transients in Fig. 2. As fitting parameters, a single value for both the coupling constant K and the initial, limiting deposition flux j_0 is used for all ionic strengths. Only the saturation coverage θ_{sat} is
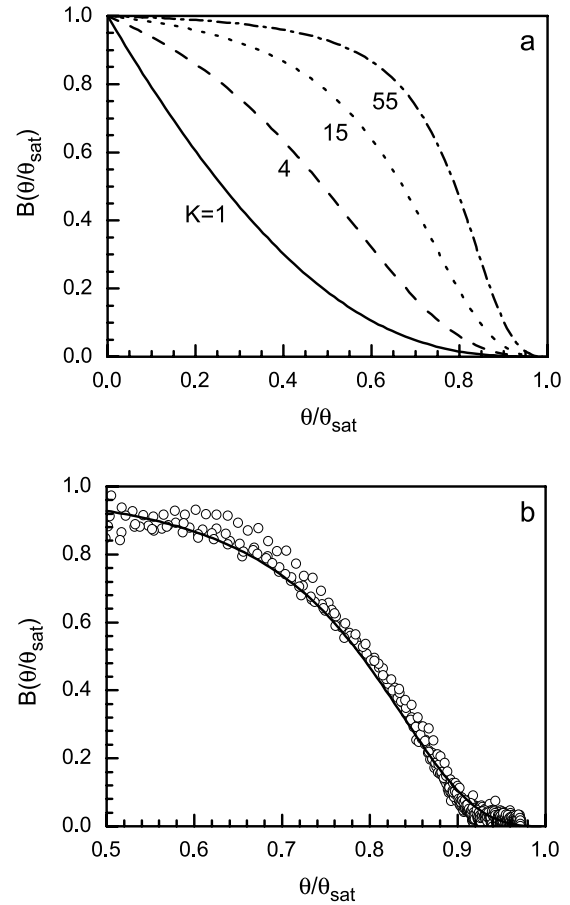

Fig. 5 (a) The overall kinetic blocking function $B(\theta/\theta_{sat})$ for different values of the coupling constant K, as a function of the normalized coverage θ/θ_{sat}. The solid line represents the RSA limit ($K=1$). The broken lines correspond to calculations using the generalized adsorption model with values for K as indicated. In (b), the data in Fig. 4 are replotted (symbols) and compared to the calculation for $K=55$.

allowed to vary with ionic strength. Over the entire coverage range, there is a perfect correspondence between the measured and calculated deposition curves. This is also shown in Fig. 5b where the data obtained from the deposition transients are compared to the overall kinetic blocking function obtained from the fits. In agreement with results presented in the previous section, the initial deposition rate $d\theta/dt = \pi a^2 j_0$ amounts to 0.0225 min^{-1}, while the saturation coverages θ_{sat} are identical to the values given in Figs. 2 and 3. The fits yield a value $K = 55 \pm 5$ for the coupling constant. Using the value $k_c = 1.44 \times 10^{-6}$ m sec^{-1} for our specific system, determined from Eq. 1, we obtain a value for the adsorption rate constant $k_a = 7.91 \times 10^{-5}$ m sec^{-1}. Using Eq. 13 with $\Delta a = 2$ nm, we obtain a value of $k_a = 2.9 \times 10^{-4}$ m sec^{-1}, somewhat higher than our experimentally determined value but of the same order of magnitude.

Comparison to Similar Nanoparticle Adsorption Experiment

Using the aforementioned generalized adsorption model, Adamczyk[48] collected adsorption rate constants for typical proteins [bovine serum albumin (BSA), fibrinogen, and IgG], which are of the same order of magnitude as our colloidal particles. Comparison with the k_a values for these proteins indicates that our aforementioned value for the irreversible deposition of nanocolloidal gold is in line with other systems of similar dimensions but of very different nature. As far as we are aware, the absolute value of the adsorption rate constant k_a has not been determined for colloidal systems with particle sizes in the low-nanometer range. In two papers,[39,53] Böhmer, Hayes, and coworkers describe similar measurements of silica particles with diameters between 32 and 200 nm. Their transients are very similar to our results for nanocolloidal gold, as presented in Fig. 2. In the analysis, the authors conclude that they are able to quantitatively analyze the limiting regimes in their deposition transients. However, the overall transients could not be adequately described.

We have taken the data from the aforementioned work and analyzed them as we have described above for gold nanocrystal adsorption. The curves all scale onto a single, universal transient, similar to our results. This is shown in Fig. 6 for a deposition experiment using silica particles with a radius $a = 16$ nm. Using Eqs. 1, 7, 11, 12, and 13, we obtain the size-dependent diffusion coefficient D and the adsorption rate constant k_a. The results are shown in Fig. 7, and compared to our results for nanocolloidal gold particles. Both the diffusion coefficient and the adsorption rate constant are lower than the trends observed for silica particles. Also, it is clear from Fig. 6 that the diffusion coefficients determined for the silica particles are in perfect agreement with the Stokes–Einstein relation
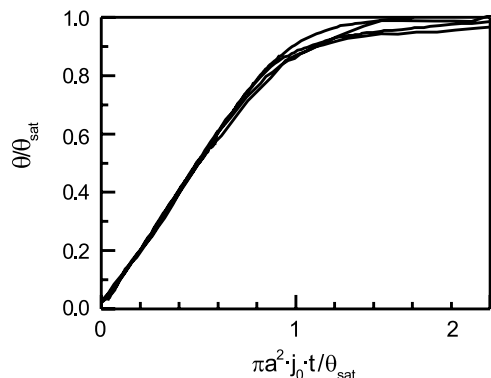

Fig. 7 Size-dependent (a) diffusion coefficient D and (b) adsorption constant k_a for silica particles, obtained from analysis of results from Refs. [39] and [53]. For comparison, the values for nanocolloidal gold from our work (solid symbol) are compared to the silica results (open symbols). The solid line in (a) represents the Stokes–Einstein relation in Eq. 2; the line in (b) is a guide to the eye.

(Eq. 2), represented by the solid line. The origin of the discrepancy between the deposition parameters of gold nanocrystals and nanocolloidal silica particles is unclear and needs further investigation.

Fig. 6 Deposition transients for 32-nm-diameter silica particles, scaled according to Eq. 9, using the dimensionless variables $\bar{\theta}$ and $\bar{t}$ as given by [Eqs. 8(a) and 8(b)] (From Ref. [39].)
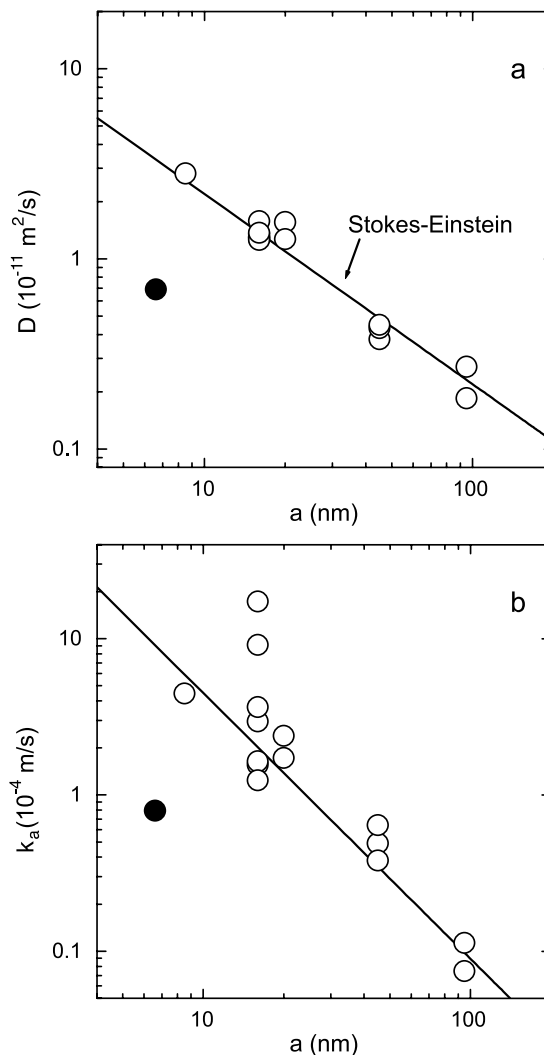
CONCLUSION

The formation of nanocolloidal thin films consisting of assembled gold nanocrystals with diameters in the low-nanometer range has been reviewed. The different methods

to produce monolayers as well as multilayered super-structures are briefly summarized.

Also, a more detailed study of the kinetics of irreversible deposition of gold nanocrystals from colloidal suspensions onto silicon/silicon oxide substrates is presented. Using a stagnation point flow geometry, the convective supply of colloidal particles is controlled. The deposition process is simultaneously monitored by in situ single wavelength reflectometry, as imaging optical methods cannot be used for such small particles. The absolute coverage is measured as a function of time for different ionic strengths. Two regimes are distinguished, related to two different processes in the adsorption process. Initially, the deposition is merely governed by mass transport limited supply of colloidal particles. The ionic strength of the suspension only affects the deposition process in the saturation regime at higher coverages.

The coupling between the convection and adsorption processes, i.e., the transition from mass transport limitation to the regime where surface blocking effects dominate, is analyzed using a generalized adsorption theory. In this theory, the deposition rate is expressed in terms of an overall kinetic blocking function. For the irreversible deposition of particles, the adsorption is treated on the basis of the random sequential adsorption model. Using the generalized adsorption model, the measured deposition curves can be adequately described, and the rate constant for particle adsorption is determined. The experimental results are compared to those for proteins and also silica particles of similar dimensions as our nanocrystals. Although there is qualitative agreement, there is a discrepancy between the results for nanocolloidal gold and the other systems. The origin of the difference is unclear.

ACKNOWLEDGMENTS

REFERENCES

1. Grabar, K.C.; Freeman, R.G.; Hommer, M.B.; Natan, M.J. Preparation and characterization of Au colloid monolayers. Anal. Chem. **1995**, *67*, 735–743.

2. Grabar, K.C.; Smith, P.C.; Musick, M.D.; Davis, J.A.; Walter, D.G.; Jackson, M.A.; Guthrie, A.P.; Natan, M.J. Kinetic control of interparticle spacing in Au colloid-based surfaces: Rational nanometer-scale architecture. J. Am. Chem. Soc. **1996**, *118*, 1148–1153.

3. Sato, T.; Ahmed, H.; Brown, D.; Johnson, B.F.G. Single electron transistor using a molecularly linked gold colloidal particle chain. J. Appl. Phys. **1997**, *82* (2), 696–701.

4. Sato, T.; Brown, D.; Johnson, B.F.G. Nucleation and growth of nano-gold colloidal lattices. Chem. Commun. **1997**, (11), 1007–1008.

5. Brust, M.; Bethell, D.; Kiely, C.J.; Schiffrin, D.J. Self-assembled gold nanoparticle thin films with nonmetallic optical and electronic properties. Langmuir **1998**, *14*, 5425–5429.

6. Schmitt, J.; Mächtle, P.; Eck, D.; Möhwald, H.; Helm, C.A. Preparation and optical properties of colloidal gold monolayers. Langmuir **1999**, *15* (9), 3256–3266.

7. Zhu, T.; Fu, X.; Mu, T.; Wang, J.; Liu, Z. pH-dependent adsorption of gold nanoparticles on *p*-aminothiophenol-modified gold substrates. Langmuir **1999**, *15* (16), 5197–5199.

8. Keating, C.D.; Musick, M.D.; Keefe, M.H.; Natan, M.J. Kinetics and thermodynamics of Au colloid monolayer self-assembly. J. Chem. Educ. **1999**, *76* (7), 949.

9. Musick, M.D.; Peña, D.J.; Botsko, S.L.; McEvoy, T.M.; Richardson, J.N.; Natan, M.J. Electrochemical properties of colloidal Au-based surfaces: Multilayer assemblies and seeded colloid films. Langmuir **1999**, *15*, 844–850.

10. Brown, K.R.; Lyon, L.A.; Fox, A.P.; Reiss, B.D.; Natan, M.J. Hydroxylamine seeded growth of colloidal Au nanoparticles. 3. Controlled formation of conductive Au films. Chem. Mater. **2000**, *12*, 314–323.

11. Shipway, A.N.; Lahav, M.; Willner, I. Nanostructured gold colloid electrodes. Adv. Mater. **2000**, *12* (13), 993–998.

12. Musick, M.D.; Keating, C.D.; Lyon, L.A.; Botsko, S.L.; Peña, D.J.; Holliway, W.D.; McEvoy, T.M.; Richardson, J.N.; Natan, M.J. Metal films prepared by stepwise assembly. 2. Construction and characterization of colloidal Au and Ag multilayers. Chem. Mater. **2000**, *12*, 2869–2881.

13. Kumar, A.; Mandale, A.B.; Sastry, M. Sequential electrostatic assembly of amine-derivatized gold and carboxylic acid-derivatized silver colloidal particles on glass substrates. Langmuir **2000**, *16*, 6921–6926.

14. Reincke, F.; Hickey, S.G.; Kelly, J.J.; Braam, T.W.; Jenneskens, L.W.; Vanmaekelbergh, D. Electrochemical and topological characterization of

gold(111)|oligo(cycolhexylidene)|gold nanocrystal interfaces. J. Electrochim. Acta **2002**, *522*, 2–10.

15. Kooij, E.S.; Brouwer, E.A.M.; Wormeester, H.; Poelsema, B. Ionic strength mediated self-organization of gold nanocrystals: An AFM study. Langmuir **2002**, *18* (20), 7677–7682.

16. Liu, S.; Zhu, T.; Hu, R.; Liu, Z. Evaporation-induced self-assembly of gold nanoparticles into a highly organized two-dimensional array. Phys. Chem. Chem. Phys. **2002**, *4*, 6059–6062.

17. Hicks, J.F.; Seok-Shon, Y.; Murray, R.W. Layer-by-layer growth of polymer/nanoparticle films containing monolayer-protected gold clusters. Langmuir **2002**, *18* (6), 2288–2294.

18. Zhang, H.L.; Evans, S.D.; Henderson, J.R. Spectroscopic ellipsometry evaluation of gold nanoparticle thin films fabricated using layer-by-layer self assembly. Adv. Mater. **2003**, *15* (6), 531–534.

19. Li, Q.; Zheng, J.; Liu, Z. Site-selective assemblies of gold nanoparticles on an AFM tip-defined silicon template. Langmuir **2003**, *19*, 166–171.

20. Cant, N.E.; Critchley, K.; Zhang, H.L.; Evans, S.D. Surface functionalization for the self-assembly of nanoparticle/polymer multilayer films. Thin Solid Films **2003**, *426*, 31–39.

21. Maeda, Y.; Tabata, H.; Kawai, T. Two-dimensional assembly of gold nanoparticles with a DNA network template. Appl. Phys. Lett. **2001**, *79* (8), 1181–1183.

22. Kumar, A.; Pattarkine, M.; Bhadbhade, M.; Mandale, A.B.; Ganesh, K.N.; Datar, S.S.; Dharmadhikari, C.V.; Sastry, M. Linear superclusters of colloidal gold particles by electrostatic assembly on DNA templates. Adv. Mater. **2001**, *13* (5), 341–344.

23. Ung, T.; Liz-Marźan, L.M.; Mulvaney, P. Optical properties of thin films of Au–SiO$_2$ particles. J. Phys. Chem., B **2001**, *105*, 3441–3452.

24. Ung, T.; Liz-Marźan, L.M.; Mulvaney, P. Gold nanoparticle thin films. Colloids Surf., A **2002**, *202*, 119–126.

25. Kolny, J.; Kornowski, A.; Weller, H. Self-organization of cadmium sulfide and gold nanoparticles by electrostatic interaction. Nano Lett. **2002**, *2* (4), 361–364.

26. Parker, A.J.; Childs, P.A.; Palmer, R.E.; Brust, M. Deposition of passivated gold nanoclusters onto prepatterned substrates. Appl. Phys. Lett. **1999**, *74* (19), 2833–2835.

27. Bailey, R.C.; Stevenson, K.J.; Hupp, J.T. Assembly of micropatterned colloidal gold thin films via microtransfer molding and electrophoretic deposition. Adv. Mater. **2000**, *12* (24), 1930–1934.

28. Giersig, M.; Mulvaney, P. Preparation of ordered colloid monolayers by electrophoretic deposition. Langmuir **1993**, *9* (12), 3408–3413.

29. Trau, M.; Saville, D.A.; Aksay, I.A. Field-induced layering of colloidal crystals. Science **1996**, *272*, 706–709.

30. Smith, P.A.; Nordquist, C.D.; Jackson, T.N.; Mayer, T.S.; Martin, B.R.; Mbindyo, J.; Mallouk, T.E. Electric-field assisted assembly and alignment of metallic nanowires. Appl. Phys. Lett. **2000**, *77* (9), 1399–1401.

31. Kim, B.; Tripp, S.L.; Wei, A. Self-organization of large gold nanoparticle arrays. J. Am. Chem. Soc. **2001**, *123*, 7955–7956.

32. Lu, Y.; Yin, Y.; Li, Z.Y.; Xia, Y. Synthesis and self-assembly of Au–SiO$_2$ core–shell colloids. Nano Lett. **2002**, *2* (7), 785–788.

33. Jana, N.R.; Gearheart, L.A.; Obare, S.O.; Johnson, C.J.; Edler, K.J.; Mann, S.; Murphy, C.J. Liquid crystalline assemblies of ordered gold nanorods. J. Mater. Chem. **2002**, *12*, 2909–2912.

34. Dijt, J.; Cohen Stuart, M.; Hofman, J.; Fleer, G. Kinetics of polymer adsorption in stagnation point flow. Colloids Surf., A **1990**, *51*, 141.

35. Kooij, E.S.; Wormeester, H.; Brouwer, E.A.M.; van Vroonhoven, E.; van Silfhout, A.; Poelsema, B. Optical characterization of thin colloidal gold films by spectroscopic ellipsometry. Langmuir **2002**, *18* (11), 4401–4413.

36. Bedeaux, D.; Vlieger, J. *Optical Properties of Surfaces*; Imperial College Press: London, 2001.

37. Dabros, T.; Van de Ven, T.G.M. A direct method for studying particle deposition onto solid surfaces. Colloid Polym. Sci. **1983**, *261*, 694–707.

38. Adamczyk, Z.; Siwek, B.; Warzyński, P.; Musia, E. Kinetics of particle deposition in the radial impinging-jet cell. J. Colloid Interface Sci. **2001**, *242*, 14–24.

39. Böhmer, M.R.; van der Zeeuw, E.A.; Koper, G.J.M. Kinetics of particle adsorption in stagnation point flow studied by optical reflectometry. J. Colloid Interface Sci. **1998**, *197* (2), 242–250.

40. Sader, J.E. Accurate analytic formulae for the far field effective potential and surface charge density of a uniform charged sphere. J. Colloid Interface Sci. **1997**, *188* (2), 508–510.

41. Yuan, Y.; Oberholzer, M.R.; Lenhoff, A.M. Size does matter: Electrostatically determined surface coverage trends in protein and colloid adsorption. Colloids Surf., A **2000**, *165* (1–3), 125–141.

42. Chow, M.K.; Zukoski, C.F. Gold sol formation mechanisms: Role of colloidal stability. J. Colloid Interface Sci. **1994**, *165* (1), 97–109.

43. Van der Zande, B.M.I.; Dhont, J.G.K.; Böhmer, M.R.; Philipse, A.P. Colloidal dispersions of gold

rods characterized by dynamic light scattering and electrophoresis. Langmuir **2000**, *16* (2), 459–464.

44. Adamczyk, Z.; Zembala, M.; Siwek, B.; Warszyński, P. Structure and ordering in localized adsorption of particles. J. Colloid Interface Sci. **1990**, *140* (1), 123–137.

45. Onoda, G.Y.; Liniger, E.G. Experimental determination of the random-parking limit in two dimensions. Phys. Rev., A **1986**, *33* (1), 715–716.

46. Schaaf, P.; Voegel, J.; Senger, B. From random sequential adsorption to ballistic deposition: A general view of irreversible deposition processes. J. Phys. Chem., B **2000**, *104* (10), 2204–2214.

47. Adamczyk, Z. Particle adsorption and deposition: Role of electrostatic interactions. Adv. Colloid Interface Sci. **2003**, *100–102*, 267–347.

48. Adamczyk, Z. Kinetics of diffusion-controlled adsorption of colloid particles and proteins. J. Colloid Interface Sci. **2000**, *229* (2), 477–489.

49. Faraudo, J.; Bafaluy, J. Distribution function approach to irreversible adsorption of interacting colloidal particles. J. Chem. Phys. **2000**, *112*, 2003–2015.

50. Adamczyk, Z.; Senger, B.; Voegel, J.; Schaaf, P. Irreversible adsorption/deposition kinetics: A generalized approach. J. Chem. Phys. **1999**, *110*, 3118–3128.

51. Schaaf, P.; Talbot, J. Surface exclusion effects in adsorption processes. J. Chem. Phys. **1989**, *91*, 4401–4409.

52. Adamczyk, Z.; Szyk, L. Kinetics of irreversible adsorption of latex particles under diffusion-controlled transport. Langmuir **2000**, *16* (13), 5730–5737.

53. Hayes, R.A.; Böhmer, M.R.; Fokkink, L.G.J. A study of silica nanoparticle adsorption using optical reflectometry and streaming potential techniques. Langmuir **1999**, *15*, 2865–2870.

Request Permission or Order Reprints Instantly!

Interested in copying and sharing this article? In most cases, U.S. Copyright Law requires that you get permission from the article's rightsholder before using copyrighted content.

All information and materials found in this article, including but not limited to text, trademarks, patents, logos, graphics and images (the "Materials"), are the copyrighted works and other forms of intellectual property of Marcel Dekker, Inc., or its licensors. All rights not expressly granted are reserved.

Get permission to lawfully reproduce and distribute the Materials or order reprints quickly and painlessly. Simply click on the "Request Permission/ Order Reprints" link below and follow the instructions. Visit the U.S. Copyright Office for information on Fair Use limitations of U.S. copyright law. Please refer to The Association of American Publishers' (AAP) website for guidelines on Fair Use in the Classroom.

The Materials are for your personal use only and cannot be reformatted, reposted, resold or distributed by electronic means or otherwise without permission from Marcel Dekker, Inc. Marcel Dekker, Inc. grants you the limited right to display the Materials only on your personal computer or personal wireless device, and to copy and download single copies of such Materials provided that any copyright, trademark or other notice appearing on such Materials is also retained by, displayed, copied or downloaded as part of the Materials and is not removed or obscured, and provided you do not edit, modify, alter or enhance the Materials. Please refer to our Website User Agreement for more details.

Request Permission/Order Reprints

Reprints of this article can also be ordered at
http://www.dekker.com/servlet/product/DOI/101081EENN120014214